Electron paramagnetic resonance of photoexcited ^{144}Nd^{3+} ion pairs in LaCl$_3$ single crystals

John M. Clemens* and Clyde A. Hutchison, Jr.

The Enrico Fermi Institute and Department of Chemistry, The University of Chicago, Chicago, Illinois 60637

The electron paramagnetic resonance spectrum of photoexcited nearest-neighbor ^{144}Nd^{3+} ion pairs in LaCl$_3$ single crystals has been obtained at a microwave frequency, ~ 24.5 GHz, and a temperature, $1.3-1.8$ K. The data for four lines of these spectra are well described by the spin Hamiltonian,

$$\mathcal{H}_S = + |\mu_B| \vec{B}_0 \cdot (^1\underline{g} \cdot {}^1\mathcal{S} + {}^2\underline{g} \cdot {}^2\mathcal{S}) + {}^1\mathcal{S} \cdot \underline{K} \cdot {}^2\mathcal{S}, \quad {}^1S = {}^2S = \tfrac{1}{2}$$

in which the principal values of $^1\underline{g}$ and $^2\underline{g}$ are shifted by only very small relative amounts from those previously found for isolated ^{144}Nd^{3+} ions in their ground $^4I_{9/2}$ and their photoexcited $^4I_{15/2}$ states, respectively, in the LaCl$_3$ crystal. It is concluded that these lines originate with nearest-neighbor pairs in which one of the ions is in the ground state and the other is in the photoexcited state. The signs and magnitudes of the shifts of the g values from those for the isolated ions are accounted for by small distortions of the crystal structure in the vicinity of the photoexcited pair. The measured principal values of $\underline{K}$ are shown to arise predominantly from magnetic dipole-dipole and superexchange ion-ion interactions. The difference in the values found for the nondipolar interaction between nearest-neighbor pairs in the photoexcited $\frac{9}{2}, \frac{15}{2}$ state and in the ground $\frac{9}{2}, \frac{9}{2}$ state indicates the occurrence of a relatively large change in the size of the superexchange interaction upon photoexcitation of one of the ions.

I. INTRODUCTION

Paramagnetic trivalent rare-earth ions in single crystals have been studied extensively by magnetic resonance and optical techniques. The ground electronic states of these ions have been investigated by EPR (electron paramagnetic resonance) and ENDOR (electron nuclear double resonance) spectroscopy.[1] Our knowledge of their excited electronic states is derived mainly from the optical studies of Dieke[2] and his colleagues. Among such rare-earth systems studied up to the present time, Nd^{3+} in anhydrous LaCl$_3$ stands out as the only system for which parallel studies of excited states by EPR and ENDOR have been made[3–8] by use of the same techniques that were employed earlier for the ground states. In the present article we present a further development in the magnetic resonance studies of rare-earth ions in photoexcited states, namely, EPR of photoexcited pairs of Nd^{3+} ions in LaCl$_3$.[9]

Magnetic resonance investigations of Nd^{3+} in the LaCl$_3$ crystal began in our laboratory with the EPR

study of the $^4I_{9/2}$, $\mu = \frac{5}{2}$ ground state by Hutchison and Wong.[3] In these experiments Nd^{3+} ions were substituted for La^{3+} ions at ~ 0.0020 of the La^{3+} sites. At this concentration the average Nd^{3+}-Nd^{3+} separation distance is ~ 35 Å, with ~ 0.92 of the Nd^{3+} ions greater than 10 Å distant from any other Nd^{3+} ions. As a result the system provides a means for studying the interaction of the Nd^{3+} ion with a crystal field of predominantly nonmagnetic ions, in the presence of an external magnetic field.

Clarke and Hutchison[4] and Hessler and Hutchison[5] subsequently observed EPR of photoexcited Nd^{3+} in the lowest Kramers doublet of the $^4I_{13/2}$ ($\mu = \frac{1}{2}$, 3932 cm^{-1}) and $^4I_{15/2}$ ($\mu = \frac{1}{2}$, 5869 cm^{-1}) manifolds. Population of these metastable Nd^{3+} states sufficient for conventional EPR detection was achieved through the efficient transfer of energy to the Nd^{3+} from photoexcited U^{3+} incorporated at La^{3+} sites in the crystal.

Halford, Hutchison, and Llewellyn[6] investigated the ENDOR transitions of the ^{143}Nd^{3+} and ^{145}Nd^{3+} ions, both with nuclear spin $I = \frac{7}{2}$. They have

pointed out that ENDOR measurements yield precise information concerning values of nuclear moments and $\langle r^{-3} \rangle$ for f electrons in Nd^{3+}. Halford[7] studied the ENDOR of these ions in detail. More recently Hessler and Hutchison[8] have repeated these investigations for $^{143}Nd^{3+}$ and $^{145}Nd^{3+}$ in the photoexcited $J = \frac{15}{2}$ state of the ^4I term of Nd^{3+}.

EPR spectroscopy of neighboring pairs of rare-earth ions provides an opportunity to study the interactions between two rare-earth ions in a predominantly nonmagnetic environment. In $LaCl_3$ crystals with ~ 0.010 of the La^{3+} sites occupied by Nd^{3+} the average Nd^{3+}-Nd^{3+} distance is ~ 20 Å. However, ~ 0.33 of the Nd^{3+} ions have one or more Nd^{3+} neighbors within 10 Å. At this concentration the linewidth of the Nd^{3+} EPR signal is narrow enough (~ 20 G) to resolve the much weaker ion-pair EPR signals from those of the isolated single ion. At the same time the concentration of ion pairs (isolated by more than 10 Å from other Nd^{3+} ions) is great enough to distinguish pair signals from noise and any impurity signals. The ratio of the number of NN (nearest-neighbor) Nd^{3+} ion pairs to the number of La^{3+} sites is $\sim 6 \times 10^{-5}$.

Brower, Stapleton, and Brower[10] (hereafter designated BSB) and Riley, Baker, and Birgeneau[11] (hereafter designated RBB) observed and analyzed the EPR spectrum of pairs of Nd^{3+} ions occupying (a) nearest- and (b) second-nearest-neighbor cation sites, which we refer to as NN and 2NN Nd^{3+} ion pairs, respectively. Baker and Marsh[12] have extended the Nd^{3+} ion-pair studies to include EPR of coupled ions as distant as seventh-nearest neighbors with a Nd^{3+}-Nd^{3+} distance of ~ 9 Å. RBB identify the interaction between NN (4.375 Å separation) and 2NN (4.840 Å separation) pairs as due to magnetic dipole interaction and superexchange. In more distant neighbors, 3NN and greater, Baker and Marsh[12] have found that magnetic dipole interaction is the primary interaction mechanism.

We report here the observation of EPR of photoexcited NN pairs of Nd^{3+} ions in $LaCl_3$.[9] We have used the two-g spin-Hamiltonian formalism depveloped by Baker[13] and BSB to describe our experimental results. In a fit of this two-g spin Hamiltonian to our data, we obtained one g value very nearly equal to that measured for the isolated ground-state $J = \frac{9}{2}$ Nd^{3+} ion, and a second g value very nearly equal to that found for the isolated state $J = \frac{15}{2}$ Nd^{3+} ion. We refer to this two-ion system as a NN $\frac{9}{2}, \frac{15}{2}$ Nd^{3+} ion pair.

II. THE CRYSTAL SYSTEM

A. LaCl₃ crystal structure

The $LaCl_3$ crystal structure is hexagonal with space group $P6_3/m$ and with two La^{3+} ions per unit

cell.[14] The lattice parameters are $|\vec{a}| = |\vec{b}| = 7.478 \pm 0.001$ Å and $|\vec{c}| = 4.375 \pm 0.001$ Å. The point symmetry at the La^{3+} site is C_{3h}. A La^{3+} ion has two nearest cation neighbors which lie above and below the mirror plane along the c axis at the distance 4.375 Å. The second-nearest cation neighbor is 4.840 Å away and the line between the two ions of this 2NN pair makes an angle 0.350π (63.1°) with respect to the c axis. There are six second-nearest cation neighbors which are related by the threefold axis and the mirror plane.

The coordination sphere for the La^{3+} ion consists of nine nearly equidistant Cl^- ions. Three Cl^- ions lie in the mirror plane at a distance 2.97 Å from the La^{3+} ion. The remaining six Cl^- ions lie three each in the planes parallel to the mirror plane at $\pm \frac{1}{2} |\vec{c}|$. The La^{3+}-Cl^- distance for these six Cl^- ions is 2.99 Å. For a NN pair of cations in $LaCl_3$ the coordination sphere consists of 15 Cl^- ions.

B. Nd³⁺ in LaCl₃

Nd^{3+} substitutes for La^{3+} at the La^{3+} ion site in $LaCl_3$.[2,3] Its ground-state electronic configuration is well described as f^3 and its lowest-energy Russell-Saunders term as $^4I_{9/2}$. Nd^{3+} is a Kramers ion; therefore, in the absence of an external magnetic field the $LaCl_3$ crystal field reduces the tenfold degenerate $^4I_{9/2}$ term to five twofold degenerate states. The ground-state doublet is described by the crystal-field quantum number $\mu = \frac{5}{2}$ (μ is the lowest $|M_J|$ value in the linear combination of $|JM_J\rangle$ functions that describes the ground state). The twofold degenerate Kramers levels can be described by a fictitious spin with $S = \frac{1}{2}$.

The Zeeman interaction of the Nd^{3+} ions with zero nuclear spin is expressed by means of the spin Hamiltonian

$$\mathscr{H}_S = + |\mu_B| \vec{B}_0 \cdot \underline{g} \cdot \vec{\mathscr{S}} , \quad S = \frac{1}{2} , \quad (1)$$

in which $|\mu_B|$ is the Bohr magneton and $\vec{\mathscr{S}}$ is the fictitious spin operator. Spin-Hamiltonian parameters for the $^4I_{9/2}, \mu = \frac{5}{2}$ system are listed in Table I.

The first excited crystal-field state lies 115.4 cm^{-1} above the ground doublet and is not thermally populated at the temperatures of our experiments.[2] The excited J manifolds of the ^4I Nd^{3+} term lie at ~ 2000 cm^{-1} ($J = \frac{11}{2}$), ~ 4000 cm^{-1} ($J = \frac{13}{2}$), and ~ 6000 cm^{-1} ($J = \frac{15}{2}$) above the ground state. The lowest-energy crystal-field states in these excited J manifolds have lifetimes on the order of 10—100 msec at liquid-helium temperatures.[15] Photoexcitation of Nd^{3+} can produce populations in these metastable states sufficient to observe EPR by conventional techniques. These states are populated

TABLE I. Spin-Hamiltonian parameter values from EPR experiments. (Standard deviations are given in parentheses.)

Ion	State	μ	Energy/hc (cm^{-1})	$g_\parallel$	$g_\perp$	Lifetime 4.2 K (msec)
Nd^{3+}	$^4I_{9/2}$	$\frac{5}{2}$	0	3.99458(2)[a]	1.76133(14)[a]	
Nd^{3+}	$^4I_{13/2}$	$\frac{1}{2}$	3932[b]	10.1892(47)[a]	1.344 7[a]	22.3±1.6[c]
Nd^{3+}	$^4I_{15/2}$	$\frac{1}{2}$	5869[b]	9.5475(207)[a]	5.1212(11)[a]	15.7±1.1[c]
				9.5526(16)[d]	5.1210(2)[d]	
U^{3+}	$^4I_{9/2}$	$\frac{5}{2}$	0	4.153(5)[e]	1.520(2)[e]	

[a]Reference 5.
[b]Reference 2.
[c]Reference 15.
[d]Present work.
[e]Reference 3.

indirectly upon the photoexcitation of Nd^{3+} by visible light by means of the ensuing radiative and nonradiative decay processes. They can also be populated indirectly by means of energy transfer from other photoexcited species.[4] The $^4I_{13/2}$ doublet, $\mu = \frac{1}{2}$, 3932 cm^{-1}, and the $^4I_{15/2}$ doublet, $\mu = \frac{1}{2}$, 5869 cm^{-1}, are well described by the spin Hamiltonian of Eq. (1). Spin-Hamiltonian parameters and other relevant information for these states are listed in Table I. The $^4I_{11/2}$ doublet, $\mu = \frac{3}{2}$, 1974 cm^{-1}, does not satisfy the selection rule for magnetic dipole transitions, $\Delta m = \pm 1$. Thus no EPR is observed for the $J = \frac{11}{2}$ state.

C. U^{3+} with Nd^{3+} in LaCl$_3$

U^{3+} substitutes for La^{3+} at the La^{3+} ion site in LaCl$_3$.[3] It has a very strong and very broad absorption in the blue region of the visible spectrum. The U^{3+} ion is a good absorber of the Ar$^+$ laser light. Clarke and Hutchison[4] have shown that this energy is very effectively used to populate excited states of Nd^{3+} via energy transfer. EPR signals from excited states of Nd^{3+} ions in crystals containing Nd^{3+} and U^{3+} are 10—20 times more intense than the signals from the same excited Nd^{3+} states in crystals containing only Nd^{3+}.

U^{3+} with the electron configuration f^3 is the 5f series analog of Nd^{3+}. Its lowest-energy Russell-Saunders term is $^4I_{9/2}$, and in LaCl$_3$ its ground state is a Kramers doublet with $\mu = \frac{5}{2}$. U^{3+} is well described by Eq. (1) and its spin-Hamiltonian parameters are listed in Table I.

III. EXPERIMENTAL DETAILS

A. Crystals

Single crystals of LaCl$_3$ with Nd^{3+} dilutely substituted for La^{3+} were prepared from the melt by the method of Anderson and Hutchison.[16] Nd$_2$O$_3$ with fractional isotopic composition 0.9751 ^{144}Nd ($I = 0$), 0.0066 ^{143}Nd ($I = \frac{7}{2}$), 0.0085 ^{145}Nd ($I = \frac{7}{2}$), and 0.0098 other spinless Nd isotopes was obtained from Oak Ridge National Laboratory and was the starting material for the preparation of the LaCl$_3$ crystals. We refer to this Nd as ^{144}Nd.

Two boules were prepared for these experiments from La$_2$O$_3$ and ^{144}Nd$_2$O$_3$ in a melt with a mole fraction, 0.010 (0.001), of ^{144}Nd^{3+}. Natural isotopic abundance U^{3+} as UCl$_3$ was prepared from U metal by the technique of Handler and Hutchison.[17] The UCl$_3$ was introduced into the melt of one of the two boules in such amount that the mole fraction of U^{3+} in the melt was 0.003 (0.001).

LaCl$_3$ crystals cleave easily along the ac and bc planes. The intersection of two such cleavage planes clearly defines the c axis of the crystal. Crystals with the approximate linear dimensions 0.2 ×0.2×0.4 cm^3 were cleaved from the boules for these experiments. All crystals possessed good cleavage surfaces.

B. Apparatus and experimental procedures

A block diagram of the experimental apparatus is shown in Fig. 1. The microwave cavity is a right
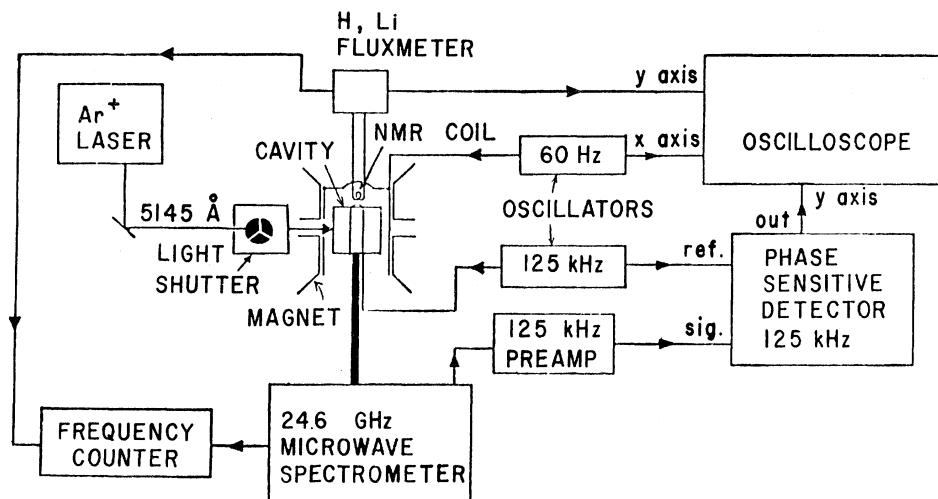
FIG. 1. Block diagram of the experimental system.

circular cylindrical cavity operating in the TE_{011} mode with a resonant frequency in the range 24.53—24.64 GHz and a Q of ~ 3000 when immersed in superfluid helium. Twenty slots were cut in the cavity wall in the bottom and on both sides to permit light to enter the cavity. Each slot is 0.020×0.635 cm^2 and is separated by 0.015 cm from the next slot. The cavity is illustrated in Fig. 2. The laboratory magnetic field, $\vec{B}_0$, is oriented perpendicular to the plane of the diagram. The microwave field, $\vec{B}_1$, lies along the axis of the cylinder. In our experiments $|\vec{B}_1|$ was 1—2 mG in the rotating frame.

The crystal samples were mounted directly on epoxy sample posts with rubber cement. The sample post was positioned along the axis of the cavity cylinder and could be rotated about this axis by a gear arrangement attached to the cavity. The angle of rotation was measured on a dial outside the cryostat. The uncertainty of angular orientation was 0.002π (0.36°). The angle between the laboratory
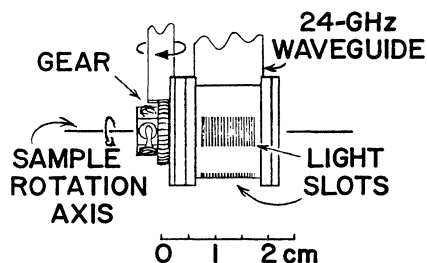
FIG. 2. Microwave cavity. The laboratory magnetic field, $\vec{B}_0$, is oriented perpendicular to the plane of the figure.

field, $\vec{B}_0$, and the c axis of the LaCl$_3$ crystal was determined by measuring the g value of the ground-state Nd^{3+} isolated-ion EPR signal.

The cavity and crystal were immersed in superfluid helium. The Dewar tailpiece had three Suprasil windows for optical experiments. The bath temperature was determined by measuring the helium vapor pressure with an oil manometer. The bath temperature during our experiments was in the range 1.3—1.8 K.

The crystals were irradiated by a cw argon-ion laser in multimode operation at a wavelength $\lambda = 5145$ Å and a power output 1 W. The laser beam was directed parallel to the laboratory magnetic field through a one-inch hole bored in the magnet pole caps. The light reached the sample after passing through the two fused silica panes of the Dewar window and the slots in the wall of the microwave cavity. Approximately half of the initial light intensity entered the cavity. Because of the arrangement for irradiating the crystal, the magnet could not be rotated. As a result the laboratory magnetic field, $\vec{B}_0$, was at all times perpendicular to the sample rotation axis. All angular variations of the crystal orientation in the magnetic field during the course of these experiments were achieved by rotation of the sample in the microwave cavity.

EPR measurements were made using conventional EPR phase-sensitive detection methods with 125-kHz field modulation of amplitude 1—5 G for EPR signals with linewidths (full width at half maximum) of ~ 10—20 G. The field strength for each EPR absorption was measured by a proton or lithium fluxmeter resonance signal. Lifetime measurements were made by simultaneously triggering a

mechanical shutter in the laser-beam path and a horizontal time sweep on a storage scope while monitoring the EPR signal intensity on the vertical axis.

IV. THE EXPERIMENTS

Experiments were performed on four crystals. Three of these crystals were cleaved from the boule with 0.010 $^{144}Nd^{3+}$ and 0.003 U^{3+} mole fractions; the fourth was cleaved from the boule containing no U^{3+}. The EPR experiments are summarized in Table II.

The microwave frequency and $|\vec{B}_0|$ for each resonance (tabulated and plotted as the frequency, ν_p, for nuclear resonance) were measured for all light-dependent EPR signals. The same light-dependent EPR spectrum was observed in all four crystals. However, only the results from crystal 3 are discussed here since they represent the most accurate of our measurments. The EPR data from crystal 3 are presented in Figs. 3 and 4. These two figures present all of the raw data for all observed light-dependent signals. The already known $^4I_{13/2}$ and $^4I_{15/2}$ spectra of isolated ions were readily recognizable and their associated points are connected by lines in the figures. Two other sets of points labeled A and B were recognizable, without data analysis, as associated with respective EPR transitions and are therefore connected by lines. Other points were associated in sets belonging to given EPR transitions only after the data analysis described below.

Figure 3 shows a plot of all the light-dependent EPR signals observed with $\vec{B}_0$ perpendicular to the c axis of the $LaCl_3$ crystal about which the crystal was rotated. The signals labeled B and $^4I_{15/2}$ display the axial symmetry of the $LaCl_3$ crystal. The $^4I_{15/2}$ signals are due to isolated $^4I_{15/2}$ Nd^{3+} and those labeled B are identified below as originating with the NN $\frac{9}{2},\frac{15}{2}$ pairs. The EPR lines labeled Y and Z display the hexagonal symmetry of the $LaCl_3$ crystal. Each one of the Z signals splits into two signals when $\vec{B}_0$ is moved out of the ab plane. These may be signals from 2NN $\frac{9}{2},\frac{15}{2}$ Nd^{3+} ion pairs.
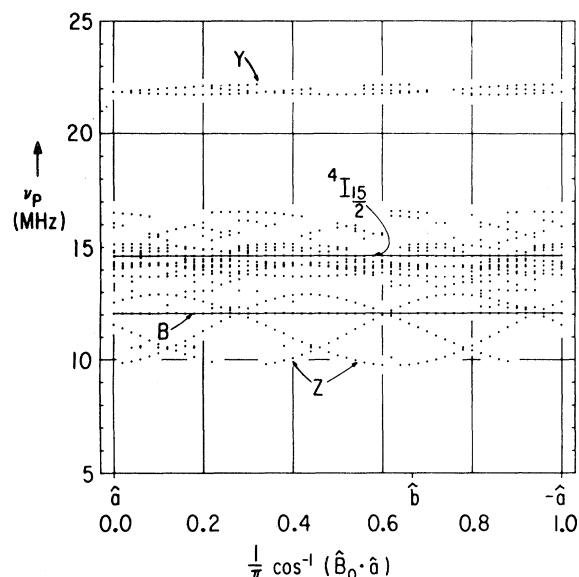

FIG. 3. Free-proton frequency for EPR vs direction of $\vec{B}_0$ in the ab plane, for light-dependent EPR signals. The sets of data labeled $^4I_{15/2}$ and B, exhibiting the axial symmetry of the crystal, are EPR of isolated $^4I_{15/2}$ Nd^{3+} ions and NN $\frac{9}{2},\frac{15}{2}$ Nd^{3+} ion pairs, respectively. The sets labeled Y and Z, reflecting the hexagonal symmetry of the crystal, are probably EPR of 2NN or 3NN $\frac{9}{2}, \frac{15}{2}$ Nd^{3+} ion pairs.

Figure 4 is a plot of the experimental data obtained with $\vec{B}_0$ lying in the crystallographic plane defined by the c axis and another principal axis, which we arbitrarily chose to call the a axis. Because of the symmetry of the EPR spectrum with respect to the c axis for $\vec{B}_0$ in the ac plane, values of ν_p for resonance were measured only for directions of $\vec{B}_0$ in this plane such that $+1 > \hat{B}_0 \cdot \hat{c} > 0$. Each measured value is plotted twice in Fig. 4, once on each side of the $\hat{a}$ abscissa. Comparison of Figs. 3 and 4 shows that the light-dependent EPR spectrum exhibits a much greater anisotropy with $\vec{B}_0$ in the

TABLE II. Summary of experiments.

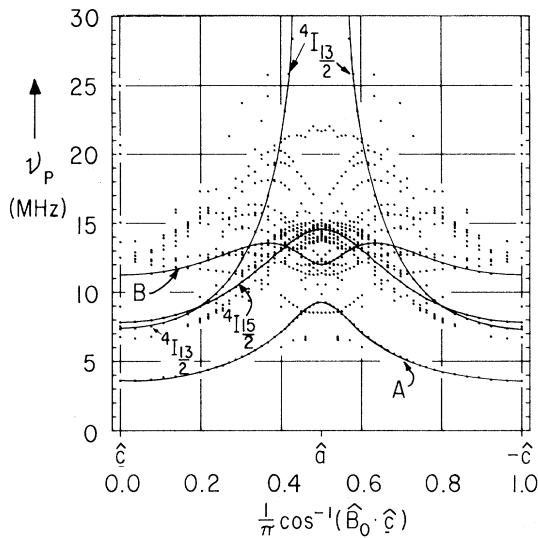| Crystal number	Axis of rotation	Number of orientations	Ions present
1	$\hat{b}$	61	$^{144}Nd^{3+}$, U^{3+}
2	$\hat{n}$	38	$^{144}Nd^{3+}$, U^{3+}
	$\frac{1}{\pi}\cos^{-1}(\hat{n}\cdot\hat{c})=0.040$		
3	$\hat{b}$	29	$^{144}Nd^{3+}$, U^{3+}
	$\hat{c}$	51	$^{144}Nd^{3+}$, U^{3+}
4	$\hat{b}$	1	$^{144}Nd^{3+}$

FIG. 4. Free-proton frequency for EPR vs direction of $\vec{B}_0$ in the ac plane, for light-dependent EPR signals. The set of data labeled A is EPR of NN $\frac{9}{2},\frac{15}{2}$ Nd^{3+} ion pairs. The labels $^4I_{13/2}$ and $^4I_{15/2}$, respectively, indicate the fields for EPR of isolated $^4I_{13/2}$ and $^4I_{15/2}$ Nd^{3+} ions at several crystal orientations.

ac plane than with $\vec{B}_0$ in the ab plane. The signals labeled A in Fig. 4 exhibit axial symmetry, but have zero intensity with $\vec{B}_0$ in the ab plane and so do not appear in Fig. 3. These EPR signals are identified below as originating with the NN $\frac{9}{2},\frac{15}{2}$ Nd^{3+} ion pairs.

Experiments were made in the field region 1—7 kG. Light-independent EPR signals, associated with ground-state Nd^{3+} and U^{3+} ions and various ion-pair combinations of these ions, prevented our observation of light-dependent EPR signals in the field region greater than 7 kG.

Finally, it is important to point out that the EPR signals from NN $\frac{9}{2},\frac{15}{2}$ Nd^{3+} ion pairs and more distant pairs of photoexcited and ground-state ions are extremely weak. The signal-to-noise ratio of the NN $\frac{9}{2},\frac{15}{2}$ Nd^{3+} EPR signals observed in our experiments was typically three or less. However, there are two factors that allowed for the precise determination of the NN $\frac{9}{2},\frac{15}{2}$ Nd^{3+} EPR data in our experiments. The first arises from the light-dependent nature of the NN $\frac{9}{2},\frac{15}{2}$ ion-pair EPR signals; in short, they flash on the oscilloscope when the photoexciting light source is chopped on and off. This allows for measurement of signals with signal-to-noise ratios of one or even less. The second point is that the g values of the $^4I_{15/2}$ Nd^{3+} ion are such that the isolated $J=\frac{15}{2}$ ion EPR signal is always well separated from the isolated ground-state Nd^{3+}

ion EPR signal. Hence a large number of the $\frac{9}{2},\frac{15}{2}$ ion-pair EPR signals occur in a field region which for the most part is free of the EPR signals from ground-state Nd^{3+} pairs (or pairs with U^{3+} ions).

V. ANALYSIS OF THE DATA

A. Identification of the NN $\frac{9}{2},\frac{15}{2}$ Nd^{3+} EPR spectrum

The EPR spectrum we observed in the Nd^{3+}-U^{3+} crystals consists of several hundred lines. Upon irradiation of the crystal by the Ar$^+$ laser, approximately twenty new EPR lines appeared which decayed upon the removal of the light.

The two most intense light-dependent signals were easily identified from their g values (see Table I) as the $^4I_{13/2}$ ($\mu=\frac{1}{2}$, 3932 cm^{-1}) and $^4I_{15/2}$ ($\mu=\frac{1}{2}$, 5869 cm^{-1}) excited-state EPR signals observed previously by Clarke and Hutchison,[4] and Hessler and Hutchison.[5] These signals were 10—100 times weaker than the ground-state ^{144}Nd^{3+} EPR signal. The remaining light-dependent EPR signals were about 10 times less intense than the $^4I_{13/2}$ and $^4I_{15/2}$ EPR lines. The angular variation in the fields for resonance of these least intense lines cannot be described by the spin Hamiltonian, (1), which applies to isolated ions.

We assigned four of the transitions associated with these least intense lines (see Fig. 5) to nearest-neighbor ^{144}Nd^{3+} ion pairs in which one of the ions was in the photoexcited $^4I_{15/2}$ state and the other was in the ground $^4I_{9/2}$ state. We based our assignment on the following four kinds of experimental observations. First, we measured at 1.5 K the $1/e$ decay times for these EPR signals and also for the isolated ion $^4I_{15/2}$ signal. They both had the same value, namely, 18(1) msec. This value is in reasonable agreement with the value, 19.5(1.1) msec, measured for the isolated ion $^4I_{15/2}$ state at 4.2 K by Gandrud and Moos.[15] Second, we found these spectra to have the axial symmetry, mentioned earlier, which must be the case for NN pairs. Third, we found that the dependence of these spectra on the direction of $\vec{B}_0$ in the crystal was excellently described by the two-g spin Hamiltonian given below in Sec. V B as would be expected for a NN pair. Fourth, some of these pair lines were observed with crystals that contained no U^{3+}, ruling out Nd^{3+}-U^{3+} or U^{3+}-U^{3+} pairs as the origins of these spectra. Thus our identification of the origin of these least intense spectra is unambiguous.
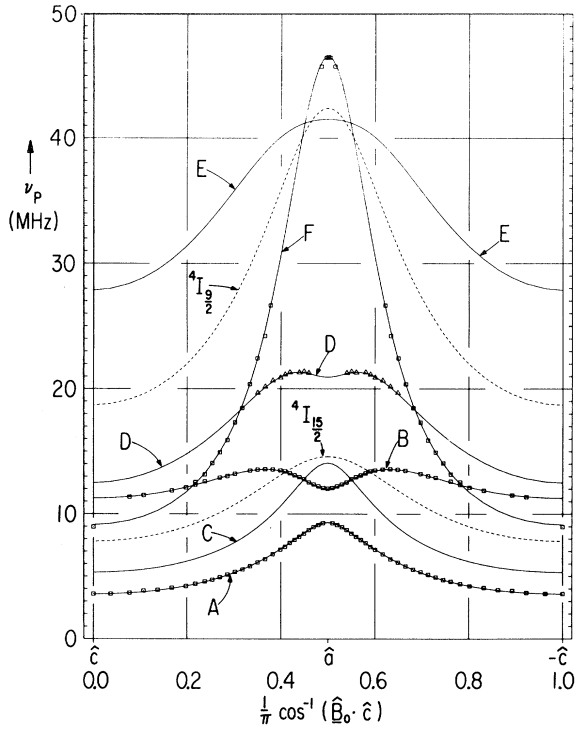
FIG. 5. Free-proton frequency for EPR vs direction of $\vec{B}_0$ in the ac plane, for NN $\frac{9}{2},\frac{15}{2}$ Nd^{3+} ion pairs. The squares and triangles are experimental data; the squares indicate the data used in the least-squares-fitting program. The solid lines are the predicted fields for NN $\frac{9}{2},\frac{15}{2}$ Nd^{3+} ion-pair EPR obtained from the least-squares best fit of Eq. (8) to the data. The labels $A-F$ refer to the transitions identified in Fig. 6. The broken-line curves are the predicted fields for EPR of isolated $^4I_{9/2}$ and $^4I_{15/2}$ Nd^{3+} ions, as labeled.

B. The spin Hamiltonian

We will describe the interaction of NN $\frac{9}{2},\frac{15}{2}$ Nd^{3+} ions with zero nuclear spin in the presence of an external magnetic field by means of the spin Hamiltonian developed by Baker[13] and BSB,

$$\mathscr{H} = \mathscr{H}_{Zeeman} + \mathscr{H}_{int} , \tag{2}$$

in which $\mathscr{H}_{Zeeman}$ is given by

$$\mathscr{H}_{Zeeman} = + |\mu_B| \vec{B}_0 \cdot {}^1\underline{g} \cdot {}^1\vec{\mathscr{S}} + |\mu_B| \vec{B}_0 \cdot {}^2\underline{g} \cdot {}^2\vec{\mathscr{S}} ,$$

$${}^1S = {}^2S = \tfrac{1}{2} , \tag{3}$$

1 and 2 index the ions of the pair, and $\mathscr{H}_{int}$ formally describes the interaction between the two ions. This interaction, consisting of dipolar, pseudodipolar, and exchange terms between two effective spins, can be written as

$$\mathscr{H}_{int} = {}^1\vec{\mathscr{S}} \cdot \underline{K} \cdot {}^2\vec{\mathscr{S}} , \quad {}^1S = {}^2S = \tfrac{1}{2} , \tag{4}$$

in which $\underline{K}$ is related to a formal second-rank symmetric tensor, $\underline{K}'$. $\underline{K}'$ is used to describe the interaction of two anisotropic spins as follows:

$$\mathscr{H}_{int} = {}^1\vec{\mathscr{S}} \cdot \underline{K} \cdot {}^2\vec{\mathscr{S}}$$
$$= ({}^1\vec{\mathscr{S}} \cdot {}^1\underline{g}) \cdot \underline{K}' \cdot ({}^2\underline{g} \cdot {}^2\vec{\mathscr{S}}) , \quad {}^1S = {}^2S = \tfrac{1}{2} . \tag{5}$$

Thus

$$\underline{K} = {}^1\underline{g} \cdot \underline{K}' {}^2\underline{g} . \tag{6}$$

We will present ${}^1\underline{g}$, ${}^2\underline{g}$, $\underline{K}'$, and vector quantities related to the spin Hamiltonian as square and column matrixes in the basis, $(\hat{u}_1,\hat{u}_2,\hat{u}_3)$, described below.

For ground-state Nd^{3+} ion pairs, when the two Nd^{3+} ions are related by inversion symmetry or the pair bond axis has twofold or higher rotation symmetry, ${}^1\underline{g} = {}^2\underline{g}$. In such a case the spin Hamiltonian can be written in terms of a singlet and triplet description. A convenient choice for $\hat{u}_3$ is then the spin precession axis, $\langle \vec{\mathscr{S}} \rangle$. A detailed discussion of this treatment is given by BSB. In working with a singlet and triplet set of bases, it is useful to decompose $\underline{K}$ into isotropic and traceless, anisotropic terms, as follows:

$$\underline{K} = J\underline{\epsilon} + \underline{A} \quad \mathrm{Tr}\underline{A} = 0 , \tag{7}$$

in which $\underline{\epsilon}$ is the unit tensor and J is the energy separation between the singlet and triplet systems. However, the selection rules for magnetic dipole transitions, $\Delta S = 0$, $\Delta m = \pm 1$, do not allow for transitions between the singlet and triplet levels. Hence in the case where the separation of the four-level system into singlet and triplet systems is exact, J is not an observable quantity. As a result the EPR spectrum for ground-state Nd^{3+} ion pairs $({}^1\underline{g} = {}^2\underline{g})$ consists of two absorption lines.

When one of the ions in the Nd^{3+} pair is photoexcited, any symmetry relationships between the two ions are broken and ${}^1\underline{g}$ and ${}^2\underline{g}$ are no longer required to be equal. As a result there is no useful singlet-triplet state description. We then take the common principal axes of ${}^1\underline{g}$ and ${}^2\underline{g}$ to be the $(\hat{u}_1,\hat{u}_2,\hat{u}_3)$ basis, in which $\hat{u}_3 = \hat{c}$ and we define $\hat{u}_2$ so as to be parallel to one of the two remaining crystallographic axes, for convenience $\hat{u}_2 \equiv \hat{b}$. EPR selection rules allow transitions between all states in the pair system, and in the case where the microwave frequency is greater in energy than the zero-field splitting of the pair system this gives a six-line EPR spectrum (see Fig. 6).

The NN Nd^{3+} ion pair in $LaCl_3$ is axially symmetric regardless of the electronic states of the Nd^{3+} ions. In our chosen basis ${}^1\underline{g}$, ${}^2\underline{g}$, and $\underline{K}'$ are diagonal with axial symmetry. $\mathscr{H}$ for NN Nd^{3+} ion pairs in $LaCl_3$ is

$$\mathscr{H} = + |\mu_B| |\vec{B}_0| [{}^1g_{||}l_3 {}^1\mathscr{S}_3 + {}^2g_{||}l_3 {}^2\mathscr{S}_3 + {}^1g_\perp(l_1 {}^1\mathscr{S}_1 + l_2 {}^1\mathscr{S}_2) + {}^2g_\perp(l_1 {}^2\mathscr{S}_1 + l_2 {}^2\mathscr{S}_2)]$$

$$+ {}^1g_\perp {}^2g_\perp K'({}^1\mathscr{S}_1 {}^2\mathscr{S}_1 + {}^1\mathscr{S}_2 {}^2\mathscr{S}_2) + {}^1g_{||} {}^2g_{||} K'_{||} {}^1\mathscr{S}_3 {}^2\mathscr{S}_3, \quad {}^1S = {}^2S = \tfrac{1}{2}. \tag{8}$$

${}^1\underline{g}$, ${}^2\underline{g}$, $\underline{K}'$, and $\vec{B}_0$ are represented in the basis, $(\hat{u}_1, \hat{u}_2, \hat{u}_3)$, by the matrices against which they are juxtaposed below;

$$
{}^1\underline{g},\quad
\begin{bmatrix}
{}^1g_\perp & 0 & 0 \\
0 & {}^1g_\perp & 0 \\
0 & 0 & {}^1g_{||}
\end{bmatrix},\quad
{}^2\underline{g},\quad
\begin{bmatrix}
{}^2g_\perp & 0 & 0 \\
0 & {}^2g_\perp & 0 \\
0 & 0 & {}^2g_{||}
\end{bmatrix},\quad
\underline{K}',\quad
\begin{bmatrix}
K'_\perp & 0 & 0 \\
0 & K'_\perp & 0 \\
0 & 0 & K'_{||}
\end{bmatrix},\quad
\text{and } \vec{B}_0,\ |\vec{B}_0|
\begin{bmatrix}
l_1 \\
l_2 \\
l_3
\end{bmatrix}. \tag{9}
$$

C. Analysis of the NN $\frac{9}{2}, \frac{15}{2}$ Nd^{3+} EPR data

In our experiments the experimental data for each EPR absorption consisted of a microwave frequency, ν_M, direction cosines of the laboratory magnetic field, l_1, l_2, l_3, and a corresponding magnetic field strength, $|\vec{B}_0|$, which we measured as a proton (or lithium) fluxmeter resonance frequency, $\nu_{p\,(\text{or Li})}$. We fixed the values of ν_M, l_1, l_2, and l_3 in a given experiment and swept the magnetic field.

We have treated ν_p as the dependent variable in the system and used the theory of Belford, Belford, and Burkhalter[18] to generate from the spin Hamiltonian (8) an eigenfield matrix, that is, a matrix whose eigenvalues are directly the proton fluxmeter frequencies for NN Nd^{3+} pair EPR lines. A least-squares best fit of the spin Hamiltonian (8) to the experimental data was achieved by adjusting, as described below, the six parameters ${}^1g_{||}$, ${}^1g_\perp$, ${}^2g_{||}$, ${}^2g_\perp$, $K'_{||}$, and $K'_\perp$ to minimize the sum of the squared deviations of the observed ν_p's from the corresponding values obtained as an eigenvalue of the eigenfield matrix.
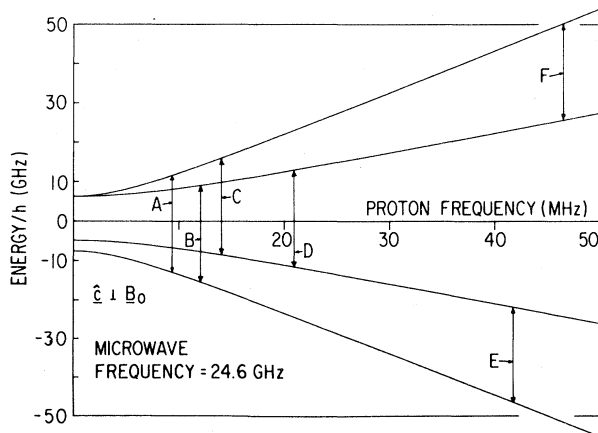
Sixty-three resonances plotted in Fig. 4, which were identified as NN $\frac{9}{2}, \frac{15}{2}$ Nd^{3+} EPR signals, were included in the least-squares fitting program. The values of ν_M, l_1, l_2, and l_3 measured for a given resonance signal were used in constructing its corresponding eigenfield matrix for each resonance used in the fitting procedure. The least-squares fitting was accomplished using a Taylor-series expansion of the observed ν_p to first order in the spin-Hamiltonian parameters. Approximate values for these parameters were refined in an iterative fashion until the sum of the squared deviations of the observed ν_p values from those calculated by the eigenfield technique was minimized. The spin Hamiltonian (8) and the resulting least-squares best-fit parameters, listed in Table III, predict the experimental ν_p values with an rms deviation of 0.068 MHz.

The fit of the spin Hamiltonian to the experimental data is shown in Fig. 5. The solid-line curves, A to F, are the predicted proton frequencies for the six EPR lines of the NN $\frac{9}{2}, \frac{15}{2}$ Nd^{3+} EPR spectrum with a microwave frequency in the range 24.53–24.64 GHz. The squares and triangles are plots of the experimental data. The triangles designate ν_p for EPR signals identified as part of the NN $\frac{9}{2}, \frac{15}{2}$ Nd^{3+} EPR spectrum after a comparison of the spin-Hamiltonian fit with the data shown in Fig. 4. The two broken-line curves are ν_p for EPR absorption as a function of the angle between B_0 and the crystal $\hat{c}$ axis for isolated Nd^{3+} ions in the ground $J = \frac{9}{2}$ and excited $J = \frac{15}{2}$ states. The letters A to F identify, respectively, the lowest-field to highest-field EPR lines in the NN $\frac{9}{2}, \frac{15}{2}$ Nd^{3+} spectrum for $\vec{B}_0$ perpendicular to $\vec{c}$. The corresponding EPR transitions are identified in the energy-level diagram shown in Fig. 6.

We calculated the relative transition probabilities, $|\langle \mathscr{S}_2 \rangle|^2$, for these spectral lines using the appropriate eigenfunctions of Eq. (8) and $\mathscr{S}_2 \equiv {}^1\mathscr{S}_2 + {}^2\mathscr{S}_2$. The results, presented in Fig. 7, agree well with the observed intensities as described below.

FIG. 6. Energy of NN $\frac{9}{2}, \frac{15}{2}$ Nd^{3+} ion-pair levels vs $|\vec{B}_0|$ given as free-proton frequency, for $\vec{B}_0$ perpendicular to $\vec{c}$.

TABLE III. NN $\frac{9}{2},\frac{15}{2}$ Nd^{3+} ion-pair spin-Hamiltonian parameters from the least-squares fit to 63 sets of experimental values. Spin-Hamiltonian parameters are also listed for ground-state NN Nd^{3+} ion pairs. (Standard deviations are given in parentheses.) Ground state NN Nd^{3+} ion-pair spin-Hamiltonian parameters from RBB (Ref. 11).

	g values for NN $\frac{9}{2},\frac{15}{2}$ Nd^{3+} ion pairs	g values for corresponding isolated ions	Δg values (column 1 minus column 2)	Ion-ion interaction parameters (cm^{-1})
$^1g_{\parallel}$	4.049(21)	3.99458(2)	+0.054	$K_{\parallel}/hc = +0.8357(97)$
$^1g_{\perp}$	1.707(9)	1.76133(14)	−0.054	$K_{\perp}/hc = -0.0905(11)$
$^2g_{\parallel}$	9.987(27)	9.5226(16)	+0.434	$J/hc = +0.2188(37)$
$^2g_{\perp}$	4.895(30)	5.1210(12)	−0.227	$A_{\parallel}/hc = +0.6176(104)$
				$A_{\perp}/hc = -0.3088(52)$

	g values for ground state NN Nd^{3+} ion pairs	g values for corresponding isolated ions	Δg values (column 1 minus column 2)	Ion-ion interaction parameters (cm^{-1})
$g_{\parallel}$	4.028(4)	3.99458(2)	+0.033	$A_{\parallel}/hc = +0.4250(80)$
$g_{\perp}$	1.717(2)	1.76133(14)	−0.044	$A_{\perp}/hc = -0.2125(40)$

The most intense EPR lines found experimentally in the NN $\frac{9}{2},\frac{15}{2}$ Nd^{3+} spectrum were those labeled A, B, and F in Fig. 5. As the crystal was rotated so that $\vec{c}$ was perpendicular to $\vec{B}_0$, the A line vanished and the B line attained a noticeable maximum in intensity, as the calculated probabilities predict. The E line, also predicted as one of the stronger spectral lines, was predicted to occur in the same magnetic field range as the ground-state Nd^{3+} and U^{3+} EPR
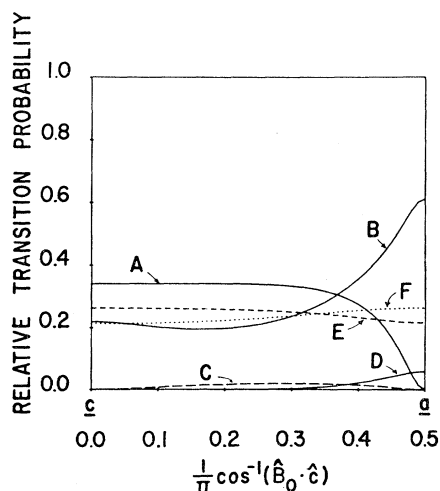
absorptions and could not be resolved from the many light-independent signals in that region. The C line is predicted to be very weak and was not observed.

VI. DISCUSSION OF THE RESULTS

EPR results for NN pairs of Nd^{3+} ions in their $J = \frac{9}{2}$ ground state have been discussed in detail by RBB. The EPR results for the NN $\frac{9}{2},\frac{15}{2}$ Nd^{3+} ion-pair system, listed in Table III, are similar in terms of the relative signs and magnitudes of the parameters to those obtained for the ground-state system. The interpretation of the EPR results for the ground-state NN Nd^{3+} ion-pair system, given by RBB, provides the framework for our discussion of the photoexcited system. They propose that for ground-state Nd^{3+} NN pairs, (a) the shifts of the g values in the spin Hamiltonian, (8), from their values for the corresponding isolated ions are due to the difference in the local crystal structure about the Nd^{3+} ion when its nearest-neighbor ion is a Nd^{3+} instead of La^{3+}, and (b) the nondipolar contribution to the ion-ion interaction term $^1\mathscr{P}\cdot\underline{K}\cdot^2\mathscr{P}$ is almost wholly due to superexchange.

These conclusions are based on a comparison of EPR results for Nd^{3+} pairs and Ce^{3+} pairs in the same crystal structure and on comparison of the results for Nd^{3+} ion pairs in the two crystals, LaCl$_3$ and LaBr$_3$, which have the same structure but different lattice constants. These comparisons are

FIG. 7. Relative probabilities for NN $\frac{9}{2},\frac{15}{2}$ Nd^{3+} ion-pair EPR transitions vs angle of $\vec{B}_0$ in the ac plane. The probabilities are labeled in accordance with Figs. 5 and 6.

motivated by the assumption that, if Ce^{3+} is substituted for Nd^{3+} or Br^- for Cl^-, the differences in the physical properties of the individual ions, viz. ionic sizes and magnetic and electric properties, can have a predictable influence on those variables of the experimental system which give rise to the observed g shifts and ion-ion interactions. The difficulty in making such comparisons is that a change from Nd^{3+} to Ce^{3+} or from Cl^- to Br^- results in a simultaneous change in many or all of these variables, namely, ion-ion distances, orbital overlap, local crystal-field distortions, and magnetic and electric effects. Our system, namely, NN $\frac{9}{2},\frac{15}{2}$ Nd^{3+} ion pairs in $LaCl_3$, provides an interesting comparison with the ground-state NN Nd^{3+} pair system in $LaCl_3$ since many of these variables are not significantly altered from one system to the other.

A. g shifts

The g values $^1g_{||}$, $^1g_\perp$, $^2g_{||}$, and $^2g_\perp$ obtained from the least-squares fit of the spin Hamiltonian to the experimental data differ from the g values for the isolated $J = \frac{9}{2}$ and $\frac{15}{2}$ Nd^{3+} ions by a small amount which we refer to as Δg. The Δg values for NN $\frac{9}{2},\frac{15}{2}$ Nd^{3+} pairs and those for the ground-state system as measured by RBB are listed in Table III.

The NN Nd^{3+} ion pair and its local structure in $LaCl_3$ consist of the unit $(Nd_2Cl_{15})^{9-}$ whereas the corresponding unit for the isolated Nd^{3+} ion is $(NdLaCl_{15})^{9-}$ (see Sec. II A). There are two important differences for a Nd^{3+} ion in these two units

(a) The nearest-neighbor cation in the ion-pair case is Nd^{3+}, a paramagnetic ion with three f electrons, and in the isolated ion case it is La^{3+}, diamagnetic and with no f electrons. The Nd^{3+}-Nd^{3+} interaction in the first case can give rise to a g shift for the Nd^{3+} ion relative to the isolated ion.

(b) Nd^{3+} is a smaller ion than La^{3+}, with an ionic radius approximately 0.93 that of La^{3+}. As a result the local crystal structure about the Nd^{3+}-Nd^{3+} ion-pair system is different from that about the Nd^{3+}-La^{3+} system. The difference in crystal structure produces a difference in the electrostatic crystal field at the Nd^{3+} ion site in the two cases. This difference in local structure can produce a g shift.

The origin of the Δg in the case of ground-state NN Nd^{3+} ion pairs has been investigated by RBB. They found that the contributions to Δg from the Nd^{3+}-Nd^{3+} interaction, as calculated by second-order perturbation theory, are too small to account for the observed Δg, primarily because the ground Kramers doublet is well separated from the first excited crystal-field states at 115 cm^{-1}. Consequently they attribute Δg to the difference of the local crys-

tal structure about the Nd^{3+} ion in an ion pair from that of an isolated ion. A comparison of NN Nd^{3+} ion pairs in $LaCl_3$ with those in $LaBr_3$ reveals a larger Δg in the tribromide case where the misfit of Nd^{3+} for La^{3+} is greater.

Because of the high symmetry of NN ion pairs in $LaCl_3$ one can construct a model for the difference in the local structures in the vicinities of the Nd^{3+} isolated ion system and the NN pair system. The observed pair EPR spectrum requires that the model for this structural distortion about the Nd^{3+} ion in the pair system maintain the axial symmetry of the pair and, from EPR results for ground-state pairs, that the model also maintain the C_{3h} symmetry of the NN Nd^{3+} pair. RBB propose that two models for this change in the local crystal structure about the Nd^{3+} ion can account for the magnitude of the Δg: (a) a displacement of the two Nd^{3+} ions towards one another along the c axis by 0.07 Å relative to the normal La^{3+} position in $LaCl_3$; (b) a displacement of the three shared Cl^- ligands toward the midpoint of the NN pair axis by 0.07 Å relative to the normal position of the Cl^- ion in $LaCl_3$.

In NN $\frac{9}{2},\frac{15}{2}$ pairs of Nd^{3+} ions one of the ions is photoexcited. The EPR results give a Δg for the ground-state $J = \frac{9}{2}$ ion which is approximately equal to that found for ground-state Nd^{3+} NN pairs, suggesting that the conclusions of RBB concerning the origin of Δg are correct. Moreover, the lowest $J = \frac{15}{2}$ doublet is well separated from the next higher crystal-field doublet (73.1 cm^{-1}), suggesting that the Nd^{3+}-Nd^{3+} interaction does not give rise to the observed Δg, as in the ground-state case. However, for the crystal-structure model to be correct, the same Nd^{3+} or Cl^- displacement that accounts for the $^4I_{9/2}$ Nd^{3+} Δg must also account for the $^4I_{15/2}$ Nd^{3+} Δg. We have examined these two models to see if any one model could account simultaneously for the Δg's we observed for both the $J = \frac{9}{2}$ and $\frac{15}{2}$ Nd^{3+} ions. This examination is described below.

The crystal-field potential at a Nd^{3+} ion site in $LaCl_3$ is given by the expansion in spherical harmonics,

$$V = \sum_{m,n} A_n^m r^n Y_n^m(\theta,\phi) . \tag{10}$$

V for f electrons in a crystal field with C_{3h} symmetry contains terms of degree $n = 2,4,6$, and $m = 0, \pm 6$. The distortion models proposed by RBB reduce the symmetry about the Nd^{3+} to C_3 in which case additional terms, $m = \pm 3$, occur in the expansion,

JOHN M. CLEMENS AND CLYDE A. HUTCHISON, JR.

$$V = A_2^0 r^2 (3 \cos^2\theta - 1) + A_4^0 r^4 (35 \cos^4\theta - 30 \cos^2\theta + 3) + A_6^0 r^6 (231 \cos^6\theta - 315 \cos^4\theta + 105 \cos^2\theta - 5)$$

$$+ A_6^6 r^6 \sin^6\theta \cos6\phi + A_4^3 r^4 \cos \sin^3\theta \cos3\phi + A_6^3 r^6 (11 \cos^3\theta - 3 \cos\theta) \sin^3\theta \cos3\phi , \tag{11}$$

in which A_6^6, A_4^3, and A_6^3 are linear combinations of the A_n^{-m} and A_n^{+m} terms from (10). For smaller deviations from Nd^{3+} C_{3h} site symmetry the A_4^3 and A_6^3 terms are expected to be small. Curtis, Newman, and Stedman[10] suggest that a distortion of the arrangement of the Cl^- ions in the Nd^{3+} coordination sphere is likely to affect only the fourth- and sixth-degree terms in (11).

We have calculated the crystal-field matrix of V and its eigenfunctions for the $J = \frac{9}{2}$ and $\frac{15}{2}$ manifolds of the ^4I term of $Nd.^{3+}$ Angular integrals of the form,

$$\langle JM_J \mid 35 \cos^4\theta - 30 \cos^2\theta + 3 \mid JM_J' \rangle ,$$

were calculated by the operator-equivalent method of Stevens.[20] The crystal-field parameters, $A_n^m \langle r^n \rangle$, were generated for $n = 4, 6$ terms using the superposition theory of Newman[21] described below.

In the superposition model the total crystal field at the Nd^{3+} ion is represented as the sum of contributions from the Cl^- ions in the Nd^{3+} coordination sphere. The contribution to the crystal-field parameter $A_n^m \langle r^n \rangle$ from the ith Cl^- ion is given by the expression,

$$\bar{A}_n (R_i) K_n^m (\theta_i, \phi_i) , \tag{12}$$

in which $\bar{A}_n (R_i)$ expresses the dependence of the contribution on the Cl^- distance from the Nd^{3+} ion

and $K_n^m (\theta_i, \phi_i)$ is an explicit function of the angular position of the ligand (a tesseral harmonic function). The crystal-field parameter is then given by the sum of the individual ligand contributions,

$$A_n^m \langle r^n \rangle = \sum_i \bar{A}_n (R_i) K_n^m (\theta_i, \phi_i) , \tag{13}$$

in which R_i, θ_i, and ϕ_i are the polar coordinates of the ligand relative to an origin at the Nd^{3+} ion and the sum runs over the 9 Cl^- ions of the Nd^{3+} coordination sphere. The $\bar{A}_n (R_i)$ parameters were obtained from crystallographic data[14] and from the crystal-field parameters of Eisenstein.[22]

From the eigenfunctions of the crystal-field matrixes, g values were calculated for the $J = \frac{9}{2}$ and $\frac{15}{2}$ states according to the relations,[1]

$$g_{\parallel} = 2\Lambda \langle + \mid \mathcal{J}_3 \mid + \rangle$$

and   (14)

$$g_{\perp} = \Lambda \langle + \mid \mathcal{J}_+ \mid - \rangle ,$$

in which Λ is the Lande factor, $\mathcal{J}_3$, $\mathcal{J}_+$ are angular momentum operators, and $\mid + \rangle$, $\mid - \rangle$ are the wave functions for the components of the Kramers doublet. Δg's were obtained from the difference of the g values calculated for Nd^{3+} in a NN ion pair and the g values calculated for an isolated Nd^{3+} ion.

The model involving a shift of the Nd^{3+} ions to-

TABLE IV. Crystal-field parameters $A_n^m \langle r^n \rangle$ calculated by the superposition theory of Newman (Ref. 21) for an isolated Nd^{3+} ion and for a Nd^{3+} ion in a NN Nd^{3+} ion pair in $LaCl_3$.

n	m	$A_n^m \langle r^n \rangle / hc$ (cm^{-1}) isolated ion (experimental)[a]	$A_n^m \langle r^n \rangle / hc$ (cm^{-1}) isolated ion (calculated)	$A_n^m \langle r^m \rangle / hc$ (cm^{-1}) NN pair ion 0.035 Å Cl^- displacement
2	0	+ 97.59	b	b
4	0	− 38.67	− 38.32	− 40.60
4	3	0	0	+ 46.71
6	0	− 44.4	− 43.81	− 45.99
6	3	0	0	+ 45.78
6	6	+ 443.	+ 428.40	+ 429.22

[a]Values given by Eisenstein (Ref. 22). [b]The $A_2^0 \langle r^2 \rangle$ parameter was not calculated, and the value given by Eisenstein was used in calculations.

TABLE V. g shifts in NN $\frac{9}{2},\frac{15}{2}$ Nd^{3+} ion pairs in $LaCl_3$.

	$^4I_{9/2}$		$^4I_{15/2}$	
	Observed	Calculated	Observed	Calculated
$\Delta g_{\parallel}$	+ 0.054	+ 0.060	+ 0.434	+ 0.378
$\Delta g_{\perp}$	− 0.054	− 0.048	− 0.227	+ 0.176

wards one another from the normal La^{3+} position produced Δg's of the wrong sign for the $^4I_{9/2}$ Nd^{3+} and values too small to account for the observed Δg's of the $^4I_{15/2}$ ion. However, the model involving a ~ 0.035-Å displacement of the shared Cl^- ligands toward the midpoint of the pair axis accounts for the sign and the magnitude of the observed Δg's for both the $J = \frac{9}{2}$ and $\frac{15}{2}$ ions. The calculation is summarized in Tables IV and V.

Our calculation of these g shifts differs from that of RBB in that we chose to consider the effect that a distortion of the Cl^- ion shell about the Nd^{3+} would have on $n = 4$ and $m = 3$ terms in the expansion of the crystal-field potential at the Nd^{3+} site. The effect of using these additional terms resulted in an optimum Cl^- displacement of approximately 0.035 Å, while consideration of only the $n = 6$, $m = 0,6$ terms required a displacement of 0.07 Å to obtain the same magnitude of Δg. We found, however, that the first model, involving a shift in the Nd^{3+} position, gives the wrong sign for both $\Delta g_{\parallel}$ and $\Delta g_{\perp}$ regardless of whether or not $n = 4$ terms are adjusted using the Newman theory or $m = 3$ terms are included in the calculation, contrary to what is reported by RBB.

In summary, our calculations suggest the following.

(a) A small distortion of the local crystal structure around the Nd^{3+} ion accounts in sign and magnitude for the Δg of both the $^4I_{9/2}$ and the $^4I_{15/2}$ Nd^{3+} ions of the ion pair.

(b) It is reasonable to assume that the predominant change in local crystal structure, on going from the isolated ion to the ion-pair system, involves a shift in the Cl^- positions and not the Nd^{3+} positions.

(c) A displacement of the three shared Cl^- ligands by ~ 0.035 Å from their normal positions in $LaCl_3$ towards the midpoint of the pair axis is reasonable. The resulting Nd-Cl and Cl-Cl distances, 2.970 and 3.478 Å, respectively, are close to those found in $NdCl_3$, namely 2.958 and 3.498 Å (in $LaCl_3$ the La-Cl distance is 2.993 Å and the Cl-Cl distance is 3.539 Å).[14]

(d) It appears that the g shift for the $^4I_{15/2}$ Nd^{3+} ion arises primarily as a result of the difference in the local structure about the Nd^{3+} ion in an ion pair

and an isolated ion.

B. The ion-ion interaction

1. Sign of the interaction tensor, $\underline{K}$

The interaction between two Nd^{3+} ions in an ion pair is represented in the spin Hamiltonian by $^1\mathscr{S}\cdot K^2\mathscr{S}$, with $^1S = {}^2S = \frac{1}{2}$. The sign of the ion-ion interaction tensor, $\underline{K}$ cannot be measured from the EPR spectrum alone. Traditional methods for determining the correct sign of the interaction involve the observation of changes in the intensities of the spectral lines with changes in temperature or with changes in the applied microwave frequency. Both of these techniques involve changing the populations of the states of a given EPR transition in a predictable fashion. Baker, Riley, and Shore[23] used these methods to identify the sign of the ion-ion interaction for the ground-state NN Nd^{3+} pair system, $A_{\parallel}/hc = 0.4250$ cm^{-1}, and $A_{\perp}/hc = -0.2125$ cm^{-1}. (See Table III.)

We have not been able to duplicate this procedure for the NN $\frac{9}{2},\frac{15}{2}$ Nd^{3+} pair system. First, we are limited in temperature variation to the superfluid helium temperature range since we photoexcite the Nd^{3+} by passing light through the liquid-helium bath. Second, we encounter problems when we change the microwave frequency from 24.6 GHz to either 9.5 or 36 GHz. At 9.5 GHz, the A and B lines in the spectrum are not observed because the zero-field splitting is greater than the microwave energy, and the F line is lost in the multitude of satellite EPR signals surrounding the $^4I_{9/2}$ single-ion resonance. At 36 GHz, the F-line resonance field is greater than 16 kG, and cannot be observed with our equipment.

We have based the choice of sign of $\underline{K}$ that appears in Table III upon the predicted and observed ratios of intensities for the B line and the F line of the EPR spectrum for $\vec{B}_0$ perpendicular to $\vec{c}$ (see Fig. 6). At this field orientation the B line is observed to be by far the most intense line in the NN $\frac{9}{2},\frac{15}{2}$ Nd^{3+} EPR spectrum. This line is $8-10$ times more intense than the F line in our experiment. The ratio of intensities of these two EPR lines can be calculated and this fact permits us to choose the

sign of the ion-ion interaction tensor, $\underline{K}$, as described below.

The ratio of intensities of two EPR lines, in our case B and F, is given by

$$\frac{I_B}{I_F} = \frac{\Delta n_B \, | \, \langle {}^B + | \, \mathscr{S}_2 \, | {}^B - \rangle \, |^2}{\Delta n_F \, | \, \langle {}^F + | \, \mathscr{S}_2 \, | {}^F - \rangle \, |^2} \, , \tag{15}$$

in which $I_{B \, (\text{or } F)}$ is the intensity of transition B (or F), $\Delta n_{B \, (\text{or } F)}$ is the difference in population of the two levels of the B (or F) transition, and

$$| \, \langle {}^{B \, (\text{or } F)} + | \, \mathscr{S}_2 \, | {}^{B \, (\text{or } F)} - \rangle \, |^2$$

is proportional to the probability for transition B (or F).

The effect of changing the sign of $\underline{K}$ is to invert the energy-level ordering of the four ion-pair states, which affects only the Δn terms in Eq. (15). Δn_B and Δn_F are easily calculated if we assume a constant number of photoexcited ion pairs, N_0, at all magnetic field strengths and a Boltzman population distribution among the energy levels of the pair system. For $\underline{K}$ with signs as listed in Table III, $\Delta n_B = 0.16 N_0$ and $N_F = 0.04 N_0$ giving a ratio of intensities, I_B/I_F, of ~ 9 at $T = 2.0$ K. For $\underline{K}$ with the opposite sign, $\Delta n_B = 0.13 N_0$, $\Delta n_F = 0.25 N_0$, and $I_B/I_F = 1.2$. The agreement of the observed ratio with the predicted ratio in the former case strongly suggests our assignment.

2. Ion-ion interaction mechanisms

For rare-earth ions in general, several ion-ion interaction mechanisms have been postulated[24]:

(a) direct coupling through orbital overlap, i.e., superexchange;

(b) direct coupling through Coulombic interaction between the nonspherical magnetic-moment distributions on the ions in the form of either magnetic multipole or electric multipole interactions;

(c) indirect coupling through the interaction of the nonspherical magnetic-moment distributions and the phonons, i.e., a virtual phonon-exchange process.

These mechanisms have been discussed extensively in the literature and a detailed review is given by Baker.[24] In the case of NN Nd^{3+} ion pairs in the ground state, RBB have identified the ion-ion in-

teraction mechanisms as magnetic dipole interaction and superexchange.

Nd^{3+} in $LaCl_3$ can be described by an anisotropic magnetic dipole moment,

$$\vec{\mu} = - \, |\mu_B| \, \underline{g} \cdot \vec{\mathscr{S}}, \quad S = \tfrac{1}{2} \, . \tag{16}$$

The separation of the Nd^{3+}-Nd^{3+} interaction into magnetic dipole and nonmagnetic dipole contributions is particularly simple as the energy of interaction between two magnetic dipole moments, ${}^1\vec{\mu}, {}^2\vec{\mu}$, separated by a distance $\vec{r}$ is given by the well-known expression,

$$\mathscr{H}_{\text{MD}} = {}^1\vec{\mu} \cdot (\underline{\epsilon} - 3\hat{r}\hat{r}) \cdot {}^2\vec{\mu} / | \, \vec{r} \, |^3 \, , \tag{17}$$

in which $\underline{\epsilon}$ is the unit dyadic and ${}^1\vec{\mu}, {}^2\vec{\mu}$ are anisotropic point dipoles of the form given in Eq. (16). For Nd^{3+} in $LaCl_3$ the magnetic dipole interaction can be calculated to within the uncertainty in the Nd^{3+}-Nd^{3+} separation in the $LaCl_3$ structure. For NN Nd^{3+} ion pairs this separation is approximately 4 Å and the radius of the Nd^{3+} ion is 0.07 Å smaller than that of the La^{3+} ion, leading to an uncertainty, ~ 0.3 Å, in the value of the Nd^{3+}-Nd^{3+} separation distance.

In calculating the magnetic dipole interaction we obtain an expression containing a linear combination of products of the g components, ${}^1g_{||} \, {}^2g_{||}$ and ${}^1g_\perp \, {}^2g_\perp$. When the interaction is between two identical ions, where ${}^1g = {}^2g$, as in the case of ground-state NN Nd^{3+} ion pairs, the sign of the products ${}^1g_{||} \, {}^2g_{||}$ and ${}^1g_\perp \, {}^2g_\perp$ is independent of the signs of the individual g components. However, when ${}^1g \neq {}^2g$, as in the case of NN $\tfrac{9}{2}, \tfrac{15}{2}$ Nd^{3+} ion pairs, the signs of the individual components enter the calculation of the magnetic dipole interaction.

If we use the spin Hamiltonian (8) to calculate the quantities we observe in an EPR experiment (not involving circularly polarized microwave radiation), we find that the signs of ${}^1g_\perp, {}^2g_\perp, {}^1g_\perp \, {}^2g_\perp, {}^1g_{||}, {}^2g_{||}$ are not observable. However, the sign of ${}^1g_{||} \, {}^2g_{||}$ is observable. Since the spin-Hamiltonian fit to our experimental data is unique, except for the ambiguity in the sign of ${}^1g_\perp \, {}^2g_\perp$, we know that ${}^1g_{||} \, {}^2g_{||}$ is positive. As a result the expression for the magnetic dipole interaction between NN $\tfrac{9}{2}, \tfrac{15}{2}$ Nd^{3+} ions can be simplified. By using Eqs. (16), (17), and $\hat{r} = \hat{u}_3$ we may obtain

$$\mathscr{H}_{\text{MD}} = \frac{+ \, |\mu_B|^2}{| \, \vec{r} \, |^3} [-2 \, | \, {}^1g_{||} \, {}^2g_{||} \, | \, {}^1\mathscr{S}_3 \, {}^2\mathscr{S}_3 \pm | \, {}^1g_\perp \, {}^2g_\perp \, | \, ({}^1\mathscr{S}_1 \, {}^2\mathscr{S}_1 + {}^1\mathscr{S}_2 \, {}^2\mathscr{S}_2)] \, , \quad {}^1S = {}^2S = \tfrac{1}{2} \, . \tag{18}$$

The ambiguity in the sign of ${}^1g_\perp \, {}^2g_\perp$ should be borne in mind throughout the discussion which follows. It arises here in the calculation of the magnetic dipole

interaction, as seen explicitly in Eq. (18), as well as in the total ion-ion interaction in $K_\perp = {}^1g_\perp \, {}^2g_\perp K'_\perp$, in which $K'_\perp$ is negative according to our discussion in

TABLE VI. Ion-ion interaction energies for NN Nd^{3+} ions in $LaCl_3$. J, $A_{||}$, and $A_\perp$ are defined by Eq. (7).

Type of ion-ion interaction	NN Nd^{3+} system	J/hc (cm^{-1})	$A_{||}/hc$ (cm^{-1})	$A_\perp/hc$ (cm^{-1})
Experimentally observed interaction	ground state	a	$+0.4250^b$ (-0.4164^c)	-0.2125^b $(+0.2082^c)$
	$\frac{9}{2},\frac{15}{2}$	$+0.2188$	$+0.6176$	-0.3088
Calculated magnetic dipole interaction	ground state	-0.0443	-0.01206	$+0.0603$
	$\frac{9}{2},\frac{15}{2}$	-0.1105	-0.3073	$+0.1536$
Residual nondipolar interaction	ground state	a	$+0.5456^b$	-0.2728^b
	$\frac{9}{2},\frac{15}{2}$	$+0.3293$	$+0.9249$	-0.4624

^{a}Not measurable.

^{b}Reference 11.

^{c}Reference 10; BSB have assumed the wrong sign for the ion-ion interaction tensor A. See Ref. 23 for a discussion of this.

Sec. VI A 1. The ambiguity has no effect on the interpretation of the results and therefore we have chosen all g values to be positive quantities for our discussion. This choice results in our using the upper (+) sign in Eq. (18) and taking K_1 to be less than zero.

The magnetic dipole interaction between the two Nd^{3+} ions in a NN ion pair is given in Table VI for ground-state and NN $\frac{9}{2},\frac{15}{2}$ Nd^{3+} ion pairs. In light of the discussion in Sec. VI A the magnetic moments, $^1\vec{\mu},^2\vec{\mu}$, were calculated from Eq. (16) using the g values given in Table III for the ion-pair spin Hamiltonian (8) rather than those for the isolated Nd^{3+} ion. A comparison of the nondipolar contribution to the Nd^{3+}-Nd^{3+} interaction for both NN Nd^{3+} pair systems is also given in Table VI.

RBB have shown that the nondipolar portion of the ion-ion interaction for ground-state Nd^{3+} pairs is wholly due to superexchange. In the following discussion we examine the possible nondipolar interaction mechanisms, i.e., electric multipole interaction, virtual phonon exchange, and superexchange, in order to determine the origin of the nondipolar part of the ion-ion interaction in NN $\frac{9}{2},\frac{15}{2}$ Nd^{3+} ion pairs and to compare this ion-ion interaction with that for ground-state and NN $\frac{9}{2},\frac{15}{2}$ Nd^{3+} ion pairs in the light of existing interaction theories.

The most general form for the ion-ion interaction Hamiltonian operating in the J manifold of the interacting ions is given by a product of Racah operators,

$$\mathcal{H}_{int}= \sum_{\substack{l,l' \\ m,m'}} \mathcal{F}_{ll'}^{mm'}\widetilde{O}_l^{m}(^1J)\widetilde{O}_{l'}^{m'}(^2J) , \qquad (19)$$

in which l,l' run over values from 0 to 6 for rare-earth ions and time-reversal symmetry requires $l+l'$ to be even. This formulation is discussed in detail by RBB, Baker,[24] and Birgeneau, Hutchings, and Rogers.[25] The axial symmetry of NN ion pairs in $LaCl_3$ requires $m = -m'$, greatly simplifying the expression for the ion-ion interaction. Evaluation of the coefficients $\mathcal{F}_{ll'}^{mm'}$ is not straightforward because of the lack of detailed understanding of the interactions or of the nature of the interacting systems for the case of electric multipole, virtual phonon, and superexchange interactions. As a result we will present here approximate values for the upper limits of the electric multipole and virtual phonon-exchange interaction contributions to the NN $\frac{9}{2},\frac{15}{2}$ Nd^{3+} ion-ion interaction to show that they are negligible as in the case of ground-state Nd^{3+} ion pairs.

The electric multipole interaction is dominated by the electric quadrupole term in the multipole expansion when the two interacting ions are separated by a distance R large compared to the distance r of the f electron from its nucleus, as is the case for our system. The electric quadrupole interaction given by Baker[24] has the form,

$$\mathcal{H}_{EQ}=\frac{e^2{}^1\chi_2{}^2\chi_2\langle^1r^2\rangle\langle^2r^2\rangle}{R^5}[6\widetilde{O}_2^0(^1J)\widetilde{O}_2^0(^2J)+4\widetilde{O}_2^1(^1J)\widetilde{O}_2^{-1}(^2J)$$

$$+4\widetilde{O}_2^{-1}(^1J)\widetilde{O}_2^1(^2J)+\widetilde{O}_2^2(^1J)\widetilde{O}_2^{-2}(^2J)+\widetilde{O}_2^{-2}(^1J)\widetilde{O}_2^2(^2J)] , \qquad (20)$$

in which the values of $\langle r^2 \rangle$ are given by Freeman and Watson,[26] $^i\chi_2$ are reduced matrix elements for the appropriate J manifold, tabulated by Stevens[20] as $\langle J||\alpha||J\rangle$, and $\tilde{O}_2^m$ are Racah operator equivalents as listed in Buckmaster.[27] This expression ignores any dielectric shielding factor, $1/\epsilon$, which takes account of the polarizability of the intervening ions in the LaCl$_3$ structure and can reduce the electric quadrupole interaction by an order of magnitude, as in the case for Ce^{3+} ion pairs in LaCl$_3$.[11,25] $1/hc$ times the electric quadrupole interaction for NN $\frac{9}{2},\frac{15}{2}$ Nd^{3+} ion pairs using Eq. (20) is $\sim 6 \times 10^{-5}$ cm^{-1} compared to $\sim 2 \times 10^{-5}$ cm^{-1} for ground-state pairs, and is negligible in comparison to the total ion-ion interaction.

The virtual phonon interaction is discussed in detail by Birgeneau, Hutchings, and Rogers.[25] Virtual phonon-exchange (VPE) coupling is a coupling of two rare-earth ions in the crystal via their respective couplings to the normal vibrational modes of the crystal. In this way the interaction Hamiltonian is expressible as a product of one-phonon orbit-lattice relaxation Hamiltonians as given by Orbach[28]

$$\mathcal{H} = \epsilon \sum_{l,m} A^m \langle r^l \rangle \chi_l \tilde{O}_l^m(J) \, , \tag{21}$$

so that the coupled interaction is expressed by

$$\mathcal{H}_{\text{VPE}} = A_{\text{VPE}} \sum_{l,l',m} A_l^m \langle r^l \rangle A_l^{-m} \langle r^{l'} \rangle {}^1\chi_l {}^2\chi_{l'}$$
$$\times \tilde{O}_l^m({}^1J) \tilde{O}_l^{-m}({}^2J) \, , \tag{22}$$

in which

$$|A_{\text{VPE}}| \approx 3 k_D C_R^2 / 2\sqrt{2}\pi^2 \rho v^2 R^2 \, ,$$

$A_l^m \langle r^l \rangle$ are the conventional static crystal-field parameters for LaCl$_3$, and the other symbols have their previously described meanings. Birgeneau, Hutchings, and Rogers[25] assign the following approximate values to the quantities in A_{VPE}:

k_D is the cutoff vector, given from a Debye temperature, ~ 190 K, as $\sim 1.2 \times 10^8$ cm^{-1};

C_R is the amount by which the orbit-lattice interaction must be scaled in order to bring the theoretical Raman relaxation time into agreement with experiment; for Nd^{3+} in LaCl$_3$, $C_R \cong 1$ (Ref. 29);

ρ is the density of LaCl$_3$; $\rho = 3.84$ gm cm^{-3};

v is the velocity of sound; $v = 2 \times 10^5$ cm sec^{-1}.

Thus a rough estimate for the value of the expression in Eq. (22) for NN $\frac{9}{2},\frac{15}{2}$ Nd^{3+} ion pairs is ~ 0.16 cm^{-1}, and since virtual phonon-exchange interaction contributes to the ion-ion interaction ten-

sor, $\underline{K}$, in second order, we find that the contribution to $\underline{K}$ from virtual phonon exchange is ~ 0.01 cm^{-1} as an upper limit. The corresponding value for ground-state Nd^{3+} ion pairs is ~ 0.001 cm^{-1}. Virtual phonon exchange seems to be more significant for NN $\frac{9}{2},\frac{15}{2}$ Nd^{3+} ion pairs than in the ground-state Nd^{3+} system. However, at most it is only 0.01 of the total nondipolar contribution to the ion-ion interaction, and we will henceforth neglect its contribution.

From the above discussion we see that ion-ion interaction in NN $\frac{9}{2},\frac{15}{2}$ Nd^{3+} ion pairs arises predominantly from magnetic dipole interaction and superexchange as is the case for the ground-state Nd^{3+} pair system. The general form of the superexchange Hamiltonian is given in Eq. (19). In this expansion the $l = l' = 0$ term corresponds to the isotropic Heisenberg exchange between two real electron spins[30]

$$\mathcal{H}_{\text{exc}} = -2J_{12} {}^1\tilde{\mathscr{S}} \cdot {}^2\tilde{\mathscr{S}} \, , \tag{23}$$

where $^1\vec{S}$ and $^2\vec{S}$ are the real spin operators in the pair system obtained from the following relations:

$$\vec{\mathscr{J}} = \vec{\mathscr{L}} + \tilde{\mathscr{S}} \, ,$$
$$\vec{\mathscr{J}} = \vec{\mathscr{L}} + 2\tilde{\mathscr{S}} = \underline{g} \cdot \vec{\mathscr{J}} \, , \tag{24}$$
$$\tilde{\mathscr{S}} = \frac{\Lambda - 1}{\Lambda} \underline{g} \cdot \vec{\mathscr{J}}, \quad S = \frac{1}{2} \, ,$$

in which Λ is the Landé factor. If we calculate the exchange interaction by Eqs. (23) and (24) we obtain $J = -2J_{12}(-1.190)$ and $A_{||} = -2J_{12}(-1.337)$. A comparison with the values listed in Table VI for the nondipolar portion of the ion-ion interaction reveals that no value of J_{12} can account for the superexchange interaction measured in our experiments. Similarly, if we calculate the exchange for ground-state pairs we obtain $A = -2J_{12}(1.245)$. A comparison of the ground-state system with the NN $\frac{9}{2},\frac{15}{2}$ system again shows that no value of J_{12} can correctly predict the magnitude of the superexchange interaction in both systems. Clearly the Heisenberg exchange interaction does not dominate the exchange between NN Nd^{3+} ions.

The difference in the nondipolar interaction between NN Nd^{3+} ions in the ground state and NN $\frac{9}{2},\frac{15}{2}$ pair systems indicates a large change in the superexchange interaction upon the photoexcitation of one of the Nd^{3+} ions. A similar result was observed by Prinz[31] in studying optical absorption line splittings in NdCl$_3$. He assumed that his observed line splittings resulted from the interaction of a photoexcited Nd^{3+} ion with its ground-state neighbors. He was able to distinguish interactions between NN Nd^{3+} ions from those between NN Nd^{3+} ions in

several different excited states. His results show a large change in the nondipolar part of the interaction between an excited Nd^{3+} ion and its ground-state neighbors depending upon the state of the excited ion.

Calculations of the superexchange interaction between two rare-earth ions have not been made from first principles. Models for superexchange require detailed information about the overlap of ligand and metal ion wave functions. A comparison of the superexchange contributions to the ion-ion interaction for Nd^{3+} ions in ground state with those for the NN $\frac{9}{2},\frac{15}{2}$ pairs indicates to some degree the sensitivity of overlap and covalency factors to the electronic states of the ions. The results of the EPR study of ground-state and NN $\frac{9}{2},\frac{15}{2}$ Nd^{3+} ion pairs provide accurate and detailed information that superexchange calculations must account for.

We can summarize our discussion of the ion-ion interaction in the NN $\frac{9}{2},\frac{15}{2}$ Nd^{3+} ion-pair system as follows.

(a) The interaction between Nd^{3+} ions in the NN $\frac{9}{2},\frac{15}{2}$ ion-pair system is almost wholly attributable to magnetic dipole interaction and superexchange as in the case of ground-state ion pairs.

(b) The superexchange interaction between two Nd^{3+} ions cannot be described by an isotropic exchange between the real ion spins in the Heisenberg exchange fashion.

(c) Our work in conjunction with the work of RBB and others serves to illustrate the sensitivity of the superexchange interaction to the angular momentum states of the interacting ions. Superexchange calculations must account for this fact.

VII. SUMMARY

We have observed the EPR spectrum of nuclear spinless NN $\frac{9}{2},\frac{15}{2}$ Nd^{3+} ion pairs in $LaCl_3$ single crystals in which one ion of the pair was photoexcited to the $^4I_{15/2}$ state and the other was in the $^4I_{9/2}$ ground state. The ion-pair spin Hamiltonian,

$$\mathcal{H}_s = + |\mu_B| \vec{B}_0 \cdot (^1\underline{g} \cdot {}^1\mathcal{S} + {}^2\underline{g} \cdot {}^2\mathcal{S})$$
$$+ {}^1\mathcal{S} \cdot \underline{K} \cdot {}^2\mathcal{S}, \quad {}^1S = {}^2S = \frac{1}{2}, \quad (25)$$

proposed by Baker[13] and BSB, gives an excellent description of the experimental data with an rms derivation, 17 G, from the measured values of $|\vec{B}_0|$ required for EPR. The g values for the least-squares best fit of (25) to the data are close to those found previously in our laboratory for the $^4I_{15/2}$ and $^4I_{9/2}$ states of single isolated Nd^{+3} ions.

From our measurements of the deviations of g values for the pairs from those for isolated ions we have shown the following. (a) A small distortion of the local crystal structure around the Nd^{3+} ion accounts in sign and magnitude for the Δg of both the $^4I_{9/2}$ and the $^4I_{15/2}$ Nd^{3+} ions of the ion pair. (b) It is reasonable to assume that the predominant change in local crystal structure, on going from the isolated ion to the ion-pair system, involves a shift in the Cl^- positions and not the Nd^{3+} positions. (c) A displacement of the three shared Cl^- ligands by ~ 0.035 Å from their normal positions in $LaCl_3$ towards the midpoint of the pair axis is reasonable. The resulting Nd-Cl and Cl-Cl distances, 2.970 and 3.478 Å, respectively, are close to those found in $NdCl_3$, namely 2.958 and 3.498 Å (in $LaCl_3$ the La-Cl distance is 2.993 Å and the Cl-Cl distance is 3.539 Å).[14] (d) The g shift for the $^4I_{15/2}$ Nd^{3+} ion arises primarily as a result of the difference in the local structure about the Nd^{3+} ion in an ion pair and an isolated ion.

From our measurements of the principal values of $\underline{K}$ in (25) and the value of J [see (7)] we have been able to draw the following conclusions. (a) The interaction between Nd^{3+} ions in the NN $\frac{9}{2}, \frac{15}{2}$ ion-pair system is almost wholly attributable to magnetic dipole interaction and superexchange as in the case of ground-state ion pairs. (b) The superexchange interaction between two Nd^{3+} ions cannot be described by an isotropic exchange between the real ion spins in the Heisenberg exchange fashion. (c) Our work in conjunction with the work of RBB and others serves to illustrate the sensitivity of the superchange interaction to the angular momentum states of the interacting ions. Superexchange calculations must account for this fact.

*Present address: Department of Chemistry, University of Pennsylvania, Philadelphia, Pennsylvania 19104.

[1]A. Abragam and B. Bleaney, *Electron Paramagnetic Resonance of Transition Ions* (Oxford University Press, Oxford, 1970).

[2]G. H. Dieke, *Spectra and Energy Levels of Rare Earth Ions in Crystals* (Wiley-Interscience, New York, 1971).

[3]C. A. Hutchison, Jr. and E. Y. Wong, J. Chem. Phys. 29, 754 (1958).

[4]R. H. Clarke and C. A. Hutchison, Jr., Phys. Rev. Lett. 27, 638 (1971).

[5]J. P. Hessler and C. A. Hutchison, Jr., Phys. Rev. B 8, 1822 (1973).

[6]D. Halford, C. A. Hutchison, Jr., and P. M. Llewellyn, Phys. Rev. 110, 284 (1958).

[7]D. Halford, Phys. Rev. 127, 1940 (1962).

[8]J. P. Hessler and C. A. Hutchison, Jr. (private communication); also see Ref. 9.

[9]A preliminary account of this work is given by C. A. Hutchison, Jr., Semicond. Insulat. 3, 61 (1978).

[10]K. L. Brower, H. J. Stapleton, and E. O. Brower, Phys. Rev. 146, 233 (1966).

[11]J. D. Riley, J. M. Baker, and R. J. Birgeneau, Proc. R. Soc. (London) Ser. A 320, 369 (1970).

[12]J. M. Baker and D. Marsh, Proc. R. Soc. London Ser. A 323, 341 (1971).

[13]J. M. Baker, Phys. Rev. 136, A1341 (1964).

[14]B. Morosin, J. Chem. Phys. 49, 3007 (1968); W. H. Zachariasen, *ibid.* 16, 254 (1948).

[15]W. B. Gandrud and H. W. Moos, J. Chem. Phys. 49, 2170 (1968).

[16]J. H. Anderson and C. A. Hutchison, Jr., Phys. Rev. 97, 76 (1955).

[17]P. Handler and C. A. Hutchison, Jr., J. Chem. Phys. 25, 1210 (1956).

[18]G. G. Belford, R. L. Belford, and J. F. Burkhalter, J. Mag. Res. 11, 251 (1973).

[19]M. M. Curtis, D. J. Newman, and G. E. Stedman, J. Chem. Phys. 50, 1077 (1969).

[20]K. W. H. Stevesn, Proc. R. Soc. (London) Ser. A 65, 209 (1952).

[21]D. J. Newman, Ad. Phys. 20, 197 (1971); D. J. Newman, Proc. Rare Earth Res. Conf. 10th 2, 1135 (1973).

[22]J. C. Eisenstein, J. Chem. Phys. 39, 2134 (1963).

[23]J. M. Baker, J. D. Riley, and R. G. Shore, Phys. Rev. 150, 198 (1966).

[24]J. M. Baker, Rep. Prog. Phys. 34, 109 (1971).

[25]R. J. Birgeneau, M. T. Hutchings, and R. N. Rogers, Phys. Rev. 175, 1116 (1968).

[26]A. J. Freeman and R. E. Watson, Phys. Rev. 127, 2058 (1962).

[27]H. A. Buckmaster, Can. J. Phys. 40, 1670 (1962).

[28]R. Orbach, Proc. R. Soc. (London) Ser. A 264, 458 (1961).

[29]C. A. Hutchison, Jr., M. D. Kemple, and Y. T. Yen, Phys. Rev. Lett. 33, 937 (1974).

[30]J. H. Van Vleck, *The Theory of Electric and Magnetic Susceptibilities* (Oxford University Press, London, 1966).

[31]G. A. Prinze, Phys. Rev. 152, 474 (1966).